MECHANICAL RESPONSE TO DEEP-CRYOGENIC TREATMENT OF ZnO NANOWIRES GROWN ON BULK ZnO COATING

MARCELLO CABIBBO[1*], DANIELE CICCARELLI[1]

[1]Dipartimento di Ingegneria Meccanica e Scienze Matematiche (DIISM), Università Politecnica delle Marche, Via Brecce Bianche, 60131 - Ancona, Italy

Abstract: ZnO nanowires are currently used in many application fields. Thermal stability is often a concern in terms of the mechanical response and, in particular, for the elasticity of the nanowires. Literature works focused, to a certain degree, on the nanowires heating response. Anyhow, no experimental data are nowadays available in literature on the low- and very low-temperature exposures. In the present study, deep-cryogenic treatment was performed on vertically aligned ZnO nanowires produced by metal organic chemical vapor deposition. The critical buckling stress and strain of individual nanowires was not significantly influenced by the cryogenic exposure, while the bulk ZnO halved.

Keywords: Deep-cryogenic treatment, ZnO nanowires, Young's modulus, Hardness, nanoindentation

1. INTRODUCTION

Zinc oxide (ZnO) has drawn considerable interest because of its semiconducting and piezoelectric properties [1-3]. In particular, ZnO nanostructures have applications as field-effect transistors [4], gas sensors [5], field-emission displays [6], and nano-electromechanical systems (NEMS) [7]. All of these applications require the knowledge and the ability to control the mechanical behavior of ZnO nanostructures. ZnO possesses one of the richest families of nanostructures: various nanorods, nanopillars, nanowires, nanodonats, nanodrums, nanopropellers, nanonails, nanobridges, nanocombs, nanorings, nanosprings, nanobelts, nanohelices, and nanocages, can be nowadays synthesized and have been widely reported in literature [3, 8]. Recently, much attention has been paid to ZnO which has self-organized one-dimensional structure: the so-called nanowires or whiskers. Nanowires (NWs) can be used in many areas, such as field emission displays, dye-sensitized solar cells, gas sensors and nanomachines [9 – 15]. They indeed constitute important semiconducting and piezoelectric materials having various applications in the field of optoelectronics [16], biosensors [17], resonators [18], electric nanogenerator [1], nanolasers [19], and nanodevices [20]. Moreover, nanostructured semiconductors such as GaN, SiC, and ZnO are of particular interest because of their applications in short wavelength light emitting devices and field emission devices [21, 22]. ZnO has some advantages over the other above mentioned nanostructures as it exhibits both semiconducting and piezoelectric properties, and it can be grown in a wide variety of geometrical configurations [19].

Due to the reported high elastic modulus and high aspect ratio [23], a further potential application of ZnO NWs is as tips for atomic force microscopy. In fact, one-dimensional (1D) oxide systems such as SnO_2 [24], tungsten oxide ($W_{18}O_{49}$) [25], GeO_2 [26], indium tin oxide (ITO) [27], Al_2O_3 [28] and ZnO [1, 29, 30] nanowires have also attracted much attention in recent years. They present the utmost challenge to semiconductor technology, making fascinating novel devices possible. It has been demonstrated that these 1D materials exhibit superior

* Corresponding author, email: m.cabibbo@univpm.it

electrical, optical, mechanical and thermal properties. It has also been shown that these materials are potential useful for nanoscale interconnects, active components of optical electronic devices and nano-electromechanical systems. For these reasons, it is important to understand mechanical characteristics of the ZnO NWs [1, 29, 30].

Presently, there are many reports on the mechanical properties of ZnO NWs [31 - 33]. For the application of NWs in NEMS, axial buckling of the NWs is a major topic of particular focus. Recent experimental findings [33] reported models to determining the buckling of ZnO NWs under uniaxial compression, and proposed a new method to observe the critical load, elastic modulus, and stress or strain of the NWs based on the Euler or Johnson buckling theory.

There are several techniques that have been developed for measuring the elastic properties of individual NW. The technique first introduced by Wong, Sheehan, Lieber [1] is based on quantifying the deflection of a single nanowire (a carbon nanotube in [1]) affixed at one end with the other end left free to be deflected by an atomic force microscope tip. The NWs were laid in parallel to a solid substrate, and the elastic modulus was calculated from the force-deflection curve.

Moreover, mechanical properties of ZnO and similar NWs have been extensively studied by tensile loading, bending, and buckling [34].

The study of nanoindentation on a vertically aligned nanowires (VANW) forest reveals a process whereby NWs are consecutively bent during the penetration of the indent tip. Therefore, the resistance of a VANW forest to penetration is due to successive bending of NWs as the tip touches the NWs. Using a micro-mechanical model of the indentation process, the effective bending stiffness of constituent NWs in the VANW array is then deduced from nanoindentation force-penetration depth curves (essentially using the classical Oliver and Pharr approach, see [35] to cite but one) [36].

Furthermore, when the size of a material is reduced to the nanoscale, owing to the large surface-to-volume ratio, surface effects will play important roles in the nanostructures. Many experimental measurements [37 - 40] have shown that the elastic property of nanostructures is markedly size-dependent, especially their lateral dimensions, which are down to several hundred nanometers or less. Among numerous models of surface effects, the theory of surface elasticity proposed by Gurtin et al. [41] has been widely employed and developed to account for the surface effects on nanoscale elements.

Different techniques have been used to grow ZnO NWs, such as laser ablation [42], chemical vapor deposition method [43], electro-deposition method [10], vapor phase transport [12], thermal evaporation using ZnO powders [29], low-temperature liquid-phase deposition [44], vapor–liquid–solid deposition [45], electrochemical decomposition, which is a less onerous technique used in industry [46], and metal organic chemical vapor deposition (MOCVD) [23, 47, 48].

In this research work, ZnO NWs were grown by MOCVD in a Si-(100) substrate. In this work, the influence of a deep cryogenic treatment on MOCVD ZnO NWs mechanical properties such Young's modulus and hardness was studied.

2. EXPERIMENTAL PROCEDURES

A vertical chamber MOCVD system was employed for the catalyst-free synthesis of the ZnO NWs. Si-(100) wafer was used as the substrate. High-purity diethyl zinc (purity > 99.99%), and N_2O (purity > 99.99%) were used as zinc and oxygen sources, respectively, and nitrogen as the carrier gas. The diethyl zinc was kept at room temperature. The working pressure of the reactor chamber was 2 kPa.

The ZnO NWs were grown via a two-step process. First, a thin nucleation layer of ZnO was grown at a temperature of 670 K. Thence, ZnO NWs were grown on the annealed nucleation layer at a temperature of 920 K and for a total duration of 30 min.

The Si/ZnO NWs samples were subjected to a cryogenic treatment consisting of a cooling from room temperature to -77 K at a rate of 1 $Kmin^{-1}$, holding at 77 K for 120 min, and slow recover to room temperature at same rate used for the cooling process.

A Hysitron© Inc. triboscope nanoindenter Ubi®-1 was used to determine the Young's modulus and hardness of the ZnO NWs prior and after a cryogenic treatment. A uniaxial compression onto the ZnO NWs was exerted by a 3-sided pyramidal Berkovich tip (with edge aperture angle of 65.35°, and radius of curvature of 150 nm). The tip and the related load function were calibrated with a fused quartz reference sample. By measuring the force-displacement curve, an average elastic modulus (i.e. Young's modulus) and hardness of each inspected material region was determined. Raw data analysis was performed according to the Oliver and Pharr method [35, 49]. A constant peak indentation force load of 1 mN was used for all the indentations.

According to the round robin experiment results reported in [49], a trapezoid load function (loading time of 20 s, holding at the peak load for 60 s, followed by 3 s unloading to the 10% of the peak load, and a final 60 s holding at this load) was here used. The hardness is given by (equation 1):

$$H = P_{max} / A_c \tag{1}$$

where P_{max} is the peak indentation load, A_c is the indentation projected contact area. The elastic modulus is given by equation 2 (a) and (b):

$$E_r = (\pi^{1/2}/2)\cdot(S/A_c^{1/2}) \tag{2a}$$

$$E_r^{-1} = (1-\nu_i^2)\cdot E_i^{-1} + (1-\nu_s^2)\cdot E_s^{-} \tag{2b}$$

where: E_r is the reduced Young's modulus (i.e. the local elastic modulus), S is the contact stiffness, which is determined from the unloading curve, E_i, E_s, ν_i, and ν_s are the elastic moduli and Poisson's ratios of the indenter and the sample, respectively. For a diamond Berkovich tip, E_i = 1040 GPa, ν_i = 0.07. A 10 x10 measurement matrix, that is, a total of 100 individual measurements, was used.

Samples surface morphology and size distribution of the NWs before and after the cryogenic treatment and the nanoindentation tests were characterized by a Zeiss© Supra®-40 field emission scanning electron microscope (FESEM), operated in an in-lens mode at 5 KV and working distances in the range 7 - 10 mm.

3. RESULTS AND DISCUSSION

Figure 1 shows a cross-section FESEM image recorded at a 30° tilt angle of the as-grown ZnO NWs. It can be seen that ZnO NWs are densely well-aligned with uniform diameter. Mean diameter, length and density of these NWs were 80 ± 5 nm, 1000 ± 80 nm, and 7.15 x$\cdot 10^9$ cm^{-2}, respectively. As shown in the Figure 1 inset, ZnO NWs were grown with an hexagonal structure.

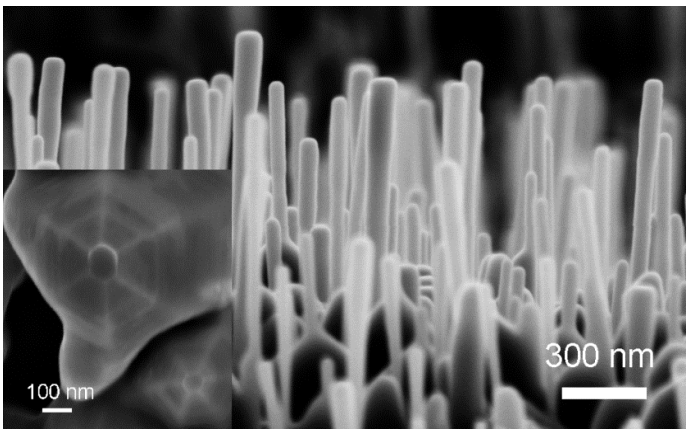

Fig. 1. Cross-section FESEM image recorded at a 30° tilt angle showing diameter, length, and distribution of the as-grown ZnO NWs. Inset is a top-view showing the grown structure of the present ZnO NWs, which are hexagonal.

Figure 2 reports a top-view FESEM micrograph of the deep-cryogenic treated NWs after nanoindentation test. It can be seen that these NWs were severely distorted and collapsed to the basement layer. Since these tests were destructive, several tests were carried out at different loads and in different ZnO NWs regions to ascertain the reproducible of the method. Results yield a full and reliable reproducibility of the method.

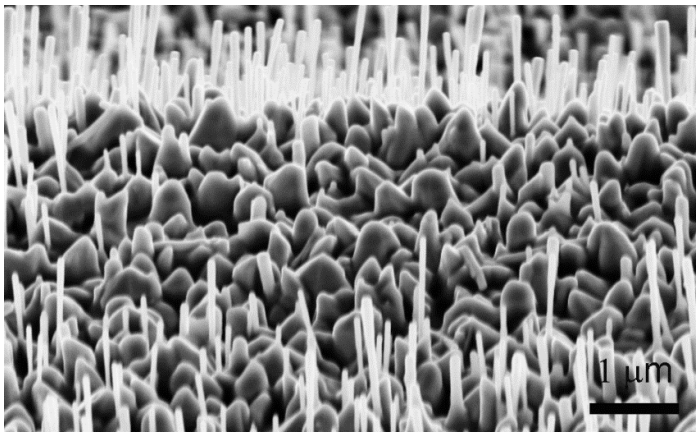

Fig. 2. FESEM top-view of the deep-cryogenic treated ZnO NWs after a nanoindentation test (applied load of 7 mN, triangular pyramidal Berkovich tip).

A typical continuous load–unload force–displacement curve for as-grown and cryogenic treated NWs is shown in Figure 3. This figure clearly illustrates that multiple discontinuities, i.e. pop-in events, in the force–displacement curves occur during loading, in both cases, the as-grown NWs (Figure 3(a)), and the deep-cryogenic treated condition (Figure 3(b)). No discontinuities have been observed on unloading. Results show that the critical load for the first pop-in, that is the elastic-plastic threshold value, essentially varies in the range of 300 - 480 μN, in both conditions. More specifically, the as-growth NWs showed a average elastic-plastic threshold load value of 390 μN, and after cryogenic treatment this mean value was of 410 μN, that is, the mean critical load did not changed significantly after cryogenic treatment. In either cases, varying the applied load (in the range of 1 to 3.5 mN) the analysis of nanoindentation curves also revealed that the larger the load required for the first pop-in to occur, the larger the length of indenter excursion during the pop-in event, i.e. larger penetration depth. As a result, the maximum penetration of the indenter is essentially independent of the number of pop-in events during loading.

The loading portion of the load-displacement curves consist of three stages which can be recognized by the value of the critical load, P_{cr}: an initial load regime, where the load, P, increases ($P < P_{cr}$), followed by a sudden drop in the curve slope, which eventually becomes flat at $P = P_{cr}$, and a third stage, where the load starts back to increase with the penetration depth, $P > P_{cr}$. The buckling instability occurs in the flat portion of the loading curve. It is well known that the behavior of an ideal column of NWs compressed by an axial load P can be summarized as follows: a. if $P < P_{cr}$, the column is in stable equilibrium in its straight position; b. if $P = P_{cr}$, the column is in a *neutral* equilibrium in either the straight or a slightly bent position; c. if $P > P_{cr}$, the column is in *unstable* equilibrium in its straight position and will buckle under the applied load. Such a type of buckling is called Euler buckling [50].

Figure 3 also shows large displacement versus load in the load range $P < P_{cr}$, which denotes a large flexibility of the ZnO NWs. This behavior was observed not only in the as-grown condition, but also, and surprisingly, after deep-cryogenic treatment. In particular, the value of the critical load, P_{cr}, is essentially the same in either the as-grown and cryogenic treated condition, these ranges from 300 to 480 μN, in the as-grown NWs, and from 360 to 440 μN, in the cryogenic treated condition. An interesting aspect is thus that the range of variability of the buckling critical load after cryogenic treatment is far more narrow, and limited to the upper value portion of the value range showed in the as-grown condition. The ranging values of the ZnO NWs critical load depend on the applied maximum load, and in most cases it rises with applied load, which ranged 1.0 to 3.5 mN. Moreover, the penetration depth reached to initiate the critical buckling load in the cryogenic treated ZnO NWs was the same as to the as-grown ZnO NWs. It is well known that the high flexibility of the ZnO NWs is attributed to the low

dimension of the structure. For instance, Chen et al. [20] showed that a pure single ZnO crystal of 100 nm diameter can be bent into a minimum of 1 μm diameter circle. Another reason may be due to the movement of the NWs at the ends support, as a perfect rigid support is impossible, which is thus not influenced by the cryogenic treatment.

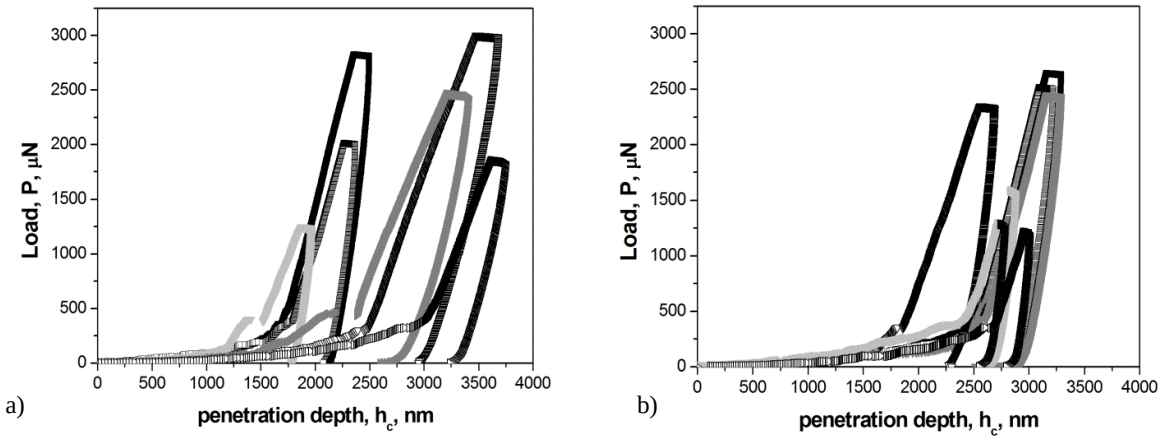

Fig. 3. Six representative load-displacement nanoindentation curves showing the pop-in event upon loading of the ZnO NWs: a) in the as-grown condition (maximum loads ranging 1.25 - to - 3.0 mN), and, b), after deep-cryogenic treatment (cooling to 77 K at a rate of 1Kmin^{-1}, holding at 77 K for 120 min, followed by 1Kmin^{-1} slow recover to room temperature), where maximum loads ranged 1.25 - to - 2.7 mN.

The FESEM top-view, reported in Figure 2, easily allows the estimation of the average critical buckling load of an individual ZnO NW. As reported in Figure 2, the area interacting with the indentation pyramidal tip is constituted by a equilateral triangle of 2 μm edge dimension (for typical applied loads of 2.5-3.5 mN), which slightly reduces to 1.7-1.8 μm in the lower load range (1.5-to-2.5 mN). The total ZnO NWs run over by the pyramidal tip are some 80. Thereafter, the critical buckling load of a single ZnO NW is about 4.9 and 5.1 μN, in the as-grown and cryogenic treated conditions, respectively. The unchanged buckling load of ZnO NWs after deep-cryogenic treatment is surely a remarkable result. This means that no change in the elastic-plastic properties of the ZnO NWs is induced by a cryogenic treatment. The obtained results, in the case of the as-grown ZnO NWs are in good agreement with other previously reported data [32, 51, 52]; in particular, in [51, 52] a critical buckling load of 5.68 μN in 2 μm-long and 100 nm-wide ZnO NWs was obtained.

Following the classical theory of elasticity of solids [53], the critical buckling load for an ideal elastic column can be expressed as (Euler load), equation (3):

$$P_{cr} = \pi^2 EI/L_{eff}^2 \tag{3}$$

where: E is the Young's modulus of an individual ZnO NW, $I = \pi D^4/32$ is the momentum of inertia, D the mean NW diameter (this taken as the outer circumference of the NW hexagonal section), L_{eff} is the effective NW length, which, for a fixed-pinned "cylindrical" NW is $0.7L$, L being the mean NW length. The critical buckling strain is given by $\varepsilon_{cr} = \sigma_{cr}/E$, where the critical buckling stress, $\sigma_{cr} = P_{cr}/A$, A being the mean section area of the hexagonal NWs ($A = (3\sqrt{3}/8)D^2$).

Table 1 compiles the values obtained for the single ZnO NW Young's modulus, E, its critical buckling stress, σ_{cr}, and strain, ε_{cr}, in the as-grown and deep-cryogenic treated conditions. The quite close Young's modulus values (86 GPa for the as-grown, and 90 GPa of the deep-cryogenic treated single ZnO NW), accounting for a slight 4% difference, clearly indicate a almost irrelevant influence of the cryogenic treatment in the elastic modulus of the ZnO NWs.

The here obtained values are reasonably close to the reported elastic modulus of single-crystal ZnO bulk coating, being E = 111 GPa as shown in [54]. The elastic properties of ZnO nanostructures and their size dependence have been previously investigated by means of transmission electron microscopy (TEM) [18, 20] and atomic

force microscopy (AFM) [50]. The Young's modulus of ZnO NWs was found to decrease dramatically with increasing diameter, reaching the ZnO bulk value for diameters typically larger than 120 nm. This behavior was attributed to a surface stiffening effect dominating at large surface-to-volume ratios [20].

Table 1. Single ZnO NW critical buckling load, P_{cr}, Young's modulus, E, stress, σ_{cr}, and strain, ε_{cr}, in the as-grown and deep-cryogenic treated conditions.

	P_{cr}, μN	E, GPa	σ_{cr}, MPa	ε_{cr}	variation, %
as-grown	4.9	86	1192	0.014	-
deep-cryogenic treated	5.1	90	1241	0.014	4

The similar critical buckling stress in both conditions also means that hardness of individual ZnO NWs is not significantly modified after cryogenic treatment.

On the other hand, Oliver and Pharr analysis of the whole load-unload curves allowed to determine the Young's modulus and hardness of the ZnO NWs prior and after deep-cryogenic treatment. Anyhow, it must be emphasized that the classical Oliver and Pharr analysis approach of the raw data allows to determine the Young's modulus and hardness of the ZnO NWs, together with the basement from which they are grown. This is due to the fact that the third part of the loading curve, i.e. for $P > P_{cr}$, pertain to the ZnO coating basement, since the NW buckling load has been exceeded. Due to the fact that the Oliver and Pharr analysis determination of the coating Young's modulus and hardness are determined from the slope, i.e. the tangent, at the starting point of the unloading curve, the obtained value derives from both ZnO base and NWs. This holds unless the substrate of Si-(100) start to contribute to the measurements. This typically holds for penetration depths approaching 20-25% of the total coating thickness. In the present case, even the maximum applied load of 3.5 mN did not reach this limit (the penetration depth being of 3500 nm, under a ZnO base thickness of 20 μm and NW of 1 μm).

Curve analysis showed that the as-grown NWs Young's modulus is $E_{as\text{-}grown}$, of 115 ± 25 GPa, which essentially doubled after deep-cryogenic treatment ($E_{post\text{-}cryo}$ = 320 ± 10 GPa). On the other hand, hardness increased slightly in the deep-cryogenic treated condition, being $H_{as\text{-}grown}$ = 4.4 ± 0.4 GPa, and $H_{post\text{-}cryo}$ = 5.3 ± 0.3 GPa. Elastic modulus and hardness of the base bulk ZnO coating well agreed with literature data (see for instance [54]). Thence, the hardness-to-elastic modulus ratio, H/E, of the ZnO coating, constituted by the base and NWs, almost was halved after cryogenic treatment. Since, as shown above, the ZnO individual stress and Young's modulus did increase of only 4% after deep-cryogenic treatment, the larger part of reduction of the Young's modulus as determined by the load-unload curve analysis is to be attributed to the bulk base ZnO coating. This indeed is an interesting result, as it was shown that, while the elastic modulus of the ZnO bulk coating halved after deep-cryogenic treatment, the ZnO NWs were practically not affected.

4. CONCLUSIONS

In summary, it was reported that deep-cryogenic treatment of MOCVD ZnO NWs did not impair the large flexibility of the as-grown ZnO NWs. It also did not influence to a significant extent the Young's modulus and the critical buckling load, stress, and strain. On the other hand, the Young's modulus of the bulk ZnO base, from which the NWs were grown, halved after the deep-cryogenic treatment.

Acknowledgements

Authors wish to thank Mrs. M. Cianci for her help in performing the cryogenic treatment and nanoindentation tests.

REFERENCES

[1] Wang, Z. L., Song, J. H., Piezoelectric nanogenerators based on zinc oxide nanowire arrays, Science, vol. 312, 2006, p. 242-6.
[2] Zhao, M.H., Wang, Z.L., Mao, S.X., Piezoelectric Characterization of Individual Zinc Oxide Nanobelt Probed by Piezoresponse Force Microscope, Nano Lett., vol. 4, 2004, p. 587-590.

[3] Wang, Z.L., Zinc oxide nanostructures: growth, properties and applications, J. Phys. Condens. Matter, vol. 16, 2004, p. 829 - 858.
[4] Wang, X., Zhou, J., Song, J., Liu, J., Xu, N., Wang, Z. L., Piezoelectric field effect transistor and nanoforce sensor based on a single ZnO nanowire, Nano Lett., vol. 6, 2006, p. 2768 - 2772.
[5] Goldberger, J., Sirbuly, D.J., Law, M., Yang, P.D., ZnO Nanowire Transistors, J. Phys. Chem. Lett. B, vol. 107, 2005, p. 9 - 14.
[6] Lee, C.J., Lee, T.J., Lyu, S.C., Zhang, Y., Ruh, H., Lee, H. J., Field emission from well-aligned zinc oxide nanowires grown at low temperature, Appl. Phys. Lett., vol. 81, 2002, p. 3648.
[7] Hughes, W. L., Wang, Z. L., Nanobelts as nanocantilevers, Appl. Phys. Lett., vol. 82, 2003, p. 2886.
[8] Djurisic, A., Ng, A., Chen, X., ZnO nanostructures for optoelectronics: Material properties and device applications, Prog. Quantum Electron., vol. 34, 2010, p. 191-259.
[9] Ataev, B.M., Kamilov, J.K., Mamedov, V.V., Zinc Oxide Whiskers, Tech. Phys. Lett., vol. 23, 1997, p. 842-845.
[10] Könenkamp, R., Boedecker, K., Lux-Steiner, M.C., Poschenrieder, M., Zenia, F., Clement, C.L., Wagner, S., Thin film semiconductor deposition on free-standing ZnO columns, Appl. Phys. Lett., vol. 77, 2000, p. 2575.
[11] Li, Y., Meng, G.W., Zhang, L.D., Ordered semiconductor ZnO nanowire arrays and their photoluminescence properties, Appl. Phys. Lett., vol. 76, 2000, p. 2011.
[12] Rao, C.N.R., Govindaraj, A., Deepak, F.L., Gunari, N.A., Nath, M., Surfactant-assisted synthesis of semiconductor nanotubes and nanowires, Appl. Phys. Lett., vol. 78, 2001, p. 1853.
[13] Huang, M.H., Mao, S., Feick, H., Yan, H., Wu, Y., Kind, H., Weber, E., Russo, R., Yang, P., Room-Temperature Ultraviolet Nanowire Nanolasers, Science, vol. 292, 2001, p. 1897-1906.
[14] Parks, W.I., Jun, Y.H., Jung, S.W., Yi, G.C., Excitonic emissions observed in ZnO single crystal nanorods, Appl. Phys. Lett., vol. 82, 2003, p. 964.
[15] Leung, Y.H., Djurišić, A.B., Choy, W.C.H., Chan, W.K., Cheah, K.W., ZnO Nanostructures Prepared by Different Methods. MRS Proceedings, vol. 818, 2004, M8.19.1.
[16] Kashif, M., Hashim, U., Ali, M.E., Usman Ali, Syed M., Rusop, M., Ibupoto, Z.H., Willander, M., Effect of Different Seed Solutions on the Morphology and Electrooptical Properties of ZnO Nanorods, J. Nanomaterials, vol.48, 2012, p. 452407.
[17] Al-Hilli, S., Öst, A., Strålfors, P., Willander, M., ZnO nanorods as an intracellular sensor for pH measurements, J. Appl. Phys., vol. 102, 2007, p. 84304.
[18] Bai, X.D., Gao, P.X., Wang, Z.L., Wang, E.G., Quantifying the elastic deformation behavior of bridged nanobelts, Appl. Phys. Lett., vol. 82, 2003, p. 4806.
[19] Zhou, H., Wissinger, M., Fallert, J., Hauschild, R., Stelzl, F., Klingshirn, C., Kalt, H., Ordered, uniform-sized ZnO nanolaser arrays, Appl. Phys. Lett.,vol. 91, 2007, p. 181112.
[20] Chen, C.Q., Shi, Y., Zhang, Y.S., Zhu, J., Yan, Y.J., Size Dependence of Young's Modulus in ZnO Nanowires, Phys. Rev. Lett., vol. 96, 2006, p. 75505.
[21] Look, D.C., Recent advances in ZnO materials and devices, Mater. Sci. Eng. B, vol. 80, 2001, p. 383-387.
[22] Muthukumar, S., Shen, H., Zhong, J., Zhang, Z., Emantoglu, N.W., Lu, Y., Selective MOCVD growth of ZnO nanotip, IEEE Trans. Nanotechnol., vol. 2, 2003, p. 50-58.
[23] Lee, W., Jeong, M.C., Myoung, J.M., Catalyst-free growth of ZnO nanowires by metal-organic chemical vapour deposition (MOCVD) and thermal evaporation, Acta Mater., vol. 52, 2004, p. 3949–3957.
[24] Dai, Z.R., Pan, Z.W., Wang, Z.L., Novel Nanostructures of Functional Oxides Synthesized by Thermal Evaporation, Adv. Funct. Mater., vol. 13, 2003, p. 9-16.
[25] Grobert N., Terrones M., Trasobares S., Kordatos K., Terrones H., Olivares J., Zhang J.P., Redlich P., Hsu W.K., Reeves C.L., Wallis D.J., Zhu Y.Q., Hare J.P., Pidduck A.J., Kroto H.W., Drm W., A novel route to aligned nanotubes and nanofibres using laser-patterned catalytic substrates, Appl. Phys. A, vol. 70, 2000, p. 175-183.
[26] Bai, Z.G., Yu, D.P., Gai, H.E.Z., Hang, Q.L., Xiong, G.C., Feng, S.Q., Nano-scale GeO_2 wires synthesized by physical evaporation, Chem. Phys. Lett., vol. 303, 1999, p. 311-315.
[27] Yumoto, H., Sako, T., Gotoh, Y., Nishiyama, K., Kaneko, T., Growth mechanism of vapor–liquid–solid (VLS) grown indium tin oxide (ITO) whiskers along the substrate, J. Cryst. Growth, vol. 203, 1999, p. 136-140.
[28] Valcarcel, V., Souto, A., Guitian, F., Development of Single-Crystal α-Al2O3 Fibers produced by Solid Deposition (VLS) from Aluminum and Powdered Silica, Adv. Mater., vol. 10, 1998, p. 138-140.
[29] Pan, Z.W., Dai, Z.R., Wang, Z.L., Nanobelts of Semiconducting Oxides, Science, vol. 291, 2001, p. 1947.
[30] Song, J.H., Wang, X.D., Riedo, E., Wang, Z.L., Elastic Property of Vertically Aligned Nanowires, Nano Lett., vol. 5, 2005, p. 1954-1962.
[31] Chen, C.Q., Zhu, J., Bending strength and flexibility of ZnO nanowires, Appl. Phys. Lett., vol. 90, 2007, p. 043105.

[32] Young, S.J., Ji, L.W., Chang, S.J., Fang, T.H., Hsueh, T.J., Meen, T.H., Chen, I.C., Nanoscale mechanical characteristics of vertical ZnO nanowires grown on ZnO:Ga/glass templates, Nanotechnology, vol. 18, 2007, p. 225603.
[33] Riaz, M., Nur, O., Willander, M., Klason, P., Buckling of ZnO nanowires under uniaxial compression, Appl. Phys. Lett., vol. 92, 2008, p. 103118.
[34] Yu, M.F., Lourie, O., Dyer, M.J., Moloni, K., Kelly, T.F., Ruoff, R.S., Strength and Breaking Mechanism of Multiwalled Carbon Nanotubes Under Tensile Load, Science, vol. 287, 2000, p. 637-40.
[35] Oliver, W.C., Pharr, G.M., An improved technique for determining hardness and elastic modulus using load and displacement sensing indentation experiments, J. Mater. Res., vol. 7, 1992, p. 1564-83.
[36] Qi, H.J., Teo, K.B.K., Lau, K.K.S., Boyce, M.C., Milne, W.I., Robertson, J., Gleason, K.K., Determination of mechanical properties of carbon nanotubes and vertically aligned carbon nanotube forests using nanoindentation, J. Mech. Phys. Solids, vol. 51, 2003, p. 2213-37.
[37] Zhu, Y., Xu, F., Qin, Q., Fung, W.Y., Lu, W., Mechanical properties of vapor - liquid - solid synthesized, silicon nanowires, Nano Lett., vol. 9, 2009, p. 3934-9.
[38] Sadeghian, H., Yang, C.K., Goosen, J.F.L., vander Drift, E., Bossche, A., French, P.J., van Keulen, F., Characterizing size-dependent effective elastic modulus of silicon nanocantilevers using electrostatic pull-in instability, Appl. Phys. Lett., vol. 94, 2009, p. 221903.
[39] Stan, G., Ciobanu, C.V., Parthangal, P.M., Cook, R.F., Diameter-dependent radial and tangential elastic moduli of ZnO nanowires, Nano Lett., vol. 7, 2007, p. 3691-3697.
[40] Asthana, A., Momeni, K., Prasad, A., Yap, Y.K., Yassar, R.S., In situ observation of size-scale effects on the mechanical properties of ZnO nanowires, Nanotechnology, vol. 22, 2011, p. 265712.
[41] Gurtin, M.E., Weissműller, J., Larché, F., A general theory of curved deformable interfaces in solids at equilibrium, Phil. Mag. A, vol. 78, 1998, p. 1093-109.
[42] Ataev, B.M., Kamilov, I.K., Mamedov, V.V., Zinc Oxide Whiskers, Tech. Phys. Lett., vol. 23, 1997, p. 842-843.
[43] Saitoh, H., Saitoh, M., Tanaka, N., Ueda, Y., Ohshio, S., Homogeneous growth of zinc oxide whiskers, Jpn. J. Appl. Phys., vol. 38 1999, p. 6873-6877.
[44] Xu, F., Yuan, Z.Y., Du, G.H., Ren, T.Z., Volcke, C., Thiry, P., Su, B.L., A low-temperature aqueous solution route to large-scale growth of ZnO nanowire arrays, J. Non-Crystal. Solids, vol. 352, 2006, p. 2569-2574.
[45] Zhang, Y.S., Yu, K., Ouyang, S.X., Zhu, Z.Q., Patterned growth and field emission of ZnO nanowires, Mater. Lett., vol. 60, 2006, p. 522-526.
[46] Leprince-Wang, Y., Wang, G.Y., Zhang, X.Z., Yu, D.P., Study on the microstructure and growth mechanism of electrochemical deposited ZnO nanowires, J. Crystal Growth, vol. 287, 2006, p. 89-93.
[47] Park, J.Y., Lee, D.J., Yun, Y.S., Moon, J.H., Lee, B.T., Kim, S.S., Temperature-induced morphological changes of ZnO grown by metalorganic chemical vapor deposition, J. Crystal Growth, vol. 276, 2005, p. 158-64.
[48] Zeng, Y.J., Ye, Z.Z., Xu, W.Z., Zhu, L.P., Zhao, B.H., Well-aligned ZnO nanowires grown on Si substrate via metal–organic chemical vapor deposition, Appl. Surf. Sci., vol. 250, 2005, p. 280-283.
[49] Cabibbo, M.; Ricci, P., Cecchini, R., Rymuza, Z.; Sullivan, J., Dub, S., Cohen, S., An international round-robin calibration protocol for nanoindentation measurements, Micron, vol. 43, 2012, p. 215-222.
[50] Mai, W.J., Wang, Z.L., Quantifying the elastic deformation behavior of bridged nanobelts, Appl. Phys. Lett., vol. 89, 2006, p. 073112.
[51] Ji, L.-W., Young, S.-J., Fang, T.-H., Liu C.-H., Buckling characterization of vertical ZnO nanowires using nanoindentation, Appl. Phys. Lett., vol. 90, 2007, p. 033109.
[52] Young, S.-J., Ji, L.-W., Chang, S.-J., Fang, T.-H., Hsueh, T.J., Nanoindentation of vertical ZnO nanowires, Physica E, vol. 39, 2007, p. 240-243.
[53] Timoshenko, S.P., Gere, J.M., Theory of Elastic Stability, McGraw-Hill, New York, 1961, p. 46.
[54] Kucheyev, S.O., Bradby, J.E., Williams, J.S., Jagadish, C., Swain, M.V., Mechanical deformation of single-crystal ZnO, Appl. Phys. Lett., vol. 80, 2002, p. 956-958.